FATIGUE AND FRACTURE OF ADDITIVELY MANUFACTURED MATERIALS

Femtosecond Laser Shock Peening Residual Stress and Fatigue Life of Additive Manufactured AlSi10Mg

JACOB BIDDLECOM, 1 YUXIN LI, 1 XIN ZHAO, 1 THOMAS A. BERFIELD, 2 and GARRETT J. PATAKY $_{\hbox{\scriptsize 10}}^{1,3}$

1.—Department of Mechanical Engineering, Clemson University, Clemson, SC 29634, USA. 2.—Department of Mechanical Engineering, University of Louisville, Louisville, KY 40292, USA. 3.—e-mail: gpataky@clemson.edu

Additive manufactured (AM) alloys are still prone to potentially critical flaws, such as gaseous bubble entrapment. These defects can lead to early crack initiation reducing fatigue life and increasing scatter, especially when near the surface. This research investigated the effect of femtosecond laser shock peening (FLSP) on the fatigue life of AM AlSi10Mg. Due to the low penetration of the FLSP, low cycle fatigue life remained consistent between treated and untreated specimens. Of equal importance though, the scatter was found to be reduced in the FLSP treated samples. From the high-resolution DIC results, the average strain per grain in the untreated specimens showed a higher increase of strain from initial loading to final fracture as compared to the FLSP samples. Implementing the use of FLSP onto AM materials could lead to more consistent fatigue life despite the presence of porosity, leading to a path of easier certification and improved confidence in their behavior.

INTRODUCTION

Additive manufacturing (AM) is becoming a wellestablished manufacturing process; however, qualification of AM parts is still as a hindrance for quickly moving parts from print to service. These issues stem from stochastic uncertainties in AM components, such as critical manufacturing flaws in the form of gaseous bubble entrapment or lack of fusion defects. 1-3 These defects can lead to premature crack initiation and early fatigue failure. This study investigated the use of laser shock peening (LSP) as a surface treatment to create a compressive stress profile into the surface beyond a critical pore depth. Both strain-controlled fatigue experiments and stress-controlled high-resolution DIC fatigue experiments were conducted to analyze the effects of surface treatment on the fatigue life of the additively manufactured aluminum alloy AlSi10Mg.

AM has become a staple in prototyping and low production run processes due to the ability to produce complex part geometries and features in a short amount of time without expensive molds.^{4,5} AM is the process in which a component is digitally sliced into layers, and each layer is printed and stacked on top of one another to create a near net shape component. ^{6,7} Many efforts have focused on ways to increase consistency in printed parts, such as the work by Jin et al. They used artificial intelligence to monitor and learn the real-time performance characteristics of an AM build process to predict where defects would occur based on the specific processing parameters at a given time.^{8–12} The two most common internal defects consist of gaseous bubble entrapment and lack of fusion voids. It has been shown that using ideal process parameters can lead to the removal of lack of fusion voids. 1,13,14 However, even with ideal processing parameters, gaseous bubble entrapment can be reduced but not removed. These defects are detrimental to the fatigue life of the components. 1-3 Considering that 90% of all component mechanical failures are due to fatigue, understanding how these defects alter the fatigue life is of the utmost importance. 15 The critical pores have been characterized in a multitude of ways including circularity, effective area, size with respect to location and distances from the surface. 3,16-19 Some studies

placed a higher emphasis on pore size, but all the studies came to a similar conclusion that the closer the defect was to the surface of the component, the more detrimental the pore was to initiating a crack during fatigue leading to fracture. ^{10,20}

With the knowledge that defects closer to the surface are more detrimental, surface treatments are well suited to combat the critical near-surface pores. Surface treatments such as shot peening and LSP have increased fatigue life on wrought materials by plastically deforming the surface of the specimens to create an area of compressive residual stress below the surface. 21-26 Both create a similar residual stress profile; however, shot peening creates a dimple-like deformed surface, which has been shown to serve as a crack initiation site during fatigue. 22,23 Laser shock peening has the potential to create a heat-affected zone that is detrimental to the material behavior, but methods have been found to mitigate them, minimizing negative effects.^{27,28} Femtosecond laser shock peeing (FLSP) can impart beneficial compressive stress while minimizing thermal damage due to its limited thermal affected zone compared to the traditional nanosecond laser shock peening (NLSP). $^{29-31}$ It was reported that the hardness improvement by FLSP is similar to or better than that of NLSP, while the affected layer depth is one order of magnitude smaller. 28 However, its effect on fatigue life was rarely studied. Sano et al. discovered that the FLSP could raise the high cycle fatigue life of aluminum alloys by 3.7 to 7 times compared to < 1 time improvement by NLSP. 32-35 Due to the ability of FLSP to target just the outer surface without altering the internal microstructure and limiting the outer damaged region, FLSP is a viable choice of surface treatment for near-net-shape AM components.

Numerous other methods have also been used to increase fatigue life of AM components. Annealing heat treatments have been shown to increase the fatigue life of specimens. ^{10,36,37} For most heat treatment cases, this result was due to the decreased residual stresses imparted during the AM process and the change of microstructure. ^{21,38} However, heat treatments have been shown to decrease the overall strength of AM materials

especially compared to wrought counterparts. ^{39–42} Hot isostatic pressing (HIP) has been shown to both decrease residual stress and remove smaller voids within the material. ^{1,7,20} Due to the high temperature and high pressure of the HIP process, some of the pores were annihilated but the microstructure of HIP specimens had greatly changed from the asprinted condition, which could lead to a decreased strength and change in overall dimensions. ^{20,43}

Although limited in number, all AM fatigue results show that LSP had a positive effect on the high cycle and above fatigue life. However, there are limited studies on the low cycle fatigue life effects of LSP on AM components. The goal of this study was to examine the effects of FLSP on additively manufactured aluminum alloy, AlSi10Mg. After the residual stress from FLSP was quantified, both strain-controlled fatigue experiments and high-resolution digital image correlation (HRDIC) were performed on as-printed and FLSP-treated samples. Although the fatigue life was not altered, the fatigue scatter was shown to decrease.

METHODS AND MATERIALS

Femto-LSP

The most common FLSP systems include a laser, scan head and stage setup. Figure 1 shows the FLSP system used where a Yb: KGW femtosecond laser source (Pharos by Light Conversion) was used to deliver laser pulses to a laser scan head (intelliSCAN by Scanlab) and an F-Theta objective lens. Table I shows all the processing parameters used during the FLSP process. The laser was applied using a raster scanning pattern. The specimens were processed under room temperature and atmospheric conditions.

Additive Manufactured AlSi10Mg

The AlSi10Mg block from which the specimens were machined was 65 mm \times 77.5 mm \times 12.3 mm. The block was manufactured on a Renishaw M250 Printer under a 200-W laser with a 70- μ m spot size at 130 μ s exposure and a striped hatch pattern. The material composition was characterized in a

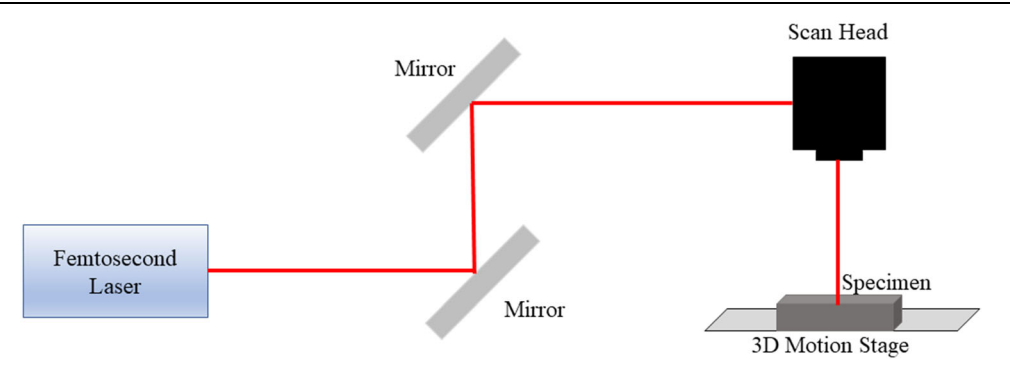


Fig. 1. Femtosecond laser shock peening system setup.

previous study and shown to be compliant with the ASTM standard. The block then was heat treated at 300°C for 2 h to alter the silicon network within the material greatly increasing ductility. Previously, experiments were performed to characterize the grain structure after heat treatment, finding there was no significant change. 44,47

To still consider the as-printed surface condition, the block was split into three sections: top, middle and bottom. Both the top and bottom sections were manufactured with a full as-printed surface on them so that when the surfaces were treated it would be representative of an as-built component surface. The specimen geometry and FLSP location are shown in Fig. 2a. The specimens were 28 mm long, 9 mm wide and between 3.4 and 4.0 mm thick. The specimens were designed so that the highest

Table I. Processing conditions for the aluminum alloy

Parameters:	Values:
Laser pulse wavelength Duration Pulse energy Laser fluence Laser focal spot size Overlapping ratio	$1030 \; \mathrm{nm}$ $165 \; \mathrm{fs}$ $1 \; \mathrm{mJ}$ $88 \; \mathrm{J/cm^2}$ $34 \; \mu \mathrm{m}$ 70%

stress would be in the middle. Due to the relatively high strain amplitudes in LCF, the catastrophic failures resulted in rough fracture surfaces causing the specimens to break outside of the field of view in some cases. Specimens were tested in the as-printed state and after FLSP. For the FLSP specimens, both flat portions of the gauge section were treated. The specimens' build location was also tracked during each experiment since there has been evidence to show that build location can also have an effect on the material response.⁴⁸

Residual Stress Analysis

A technique known as the contour method was used to determine the residual stress produced by the FSLP process. This method was adopted from the work of Prime et al. 49–51 This method is broken down into three major steps: (1) cut the specimen into sections along the cross section where the residual stress is of question; (2) take those cut surfaces and map the heights on those two surfaces using a profilometer; (3) then take those heights and use them as inputs for a finite element analysis (FEA) model that would replicate displacing those heights back to the original flat surface to calculate the residual stresses on that plane. Results of residual stress measurements via the contour method have been found to agree with neutron diffraction, with a precision of 5-20%, similar to other methods such as hole drilling and the slitting

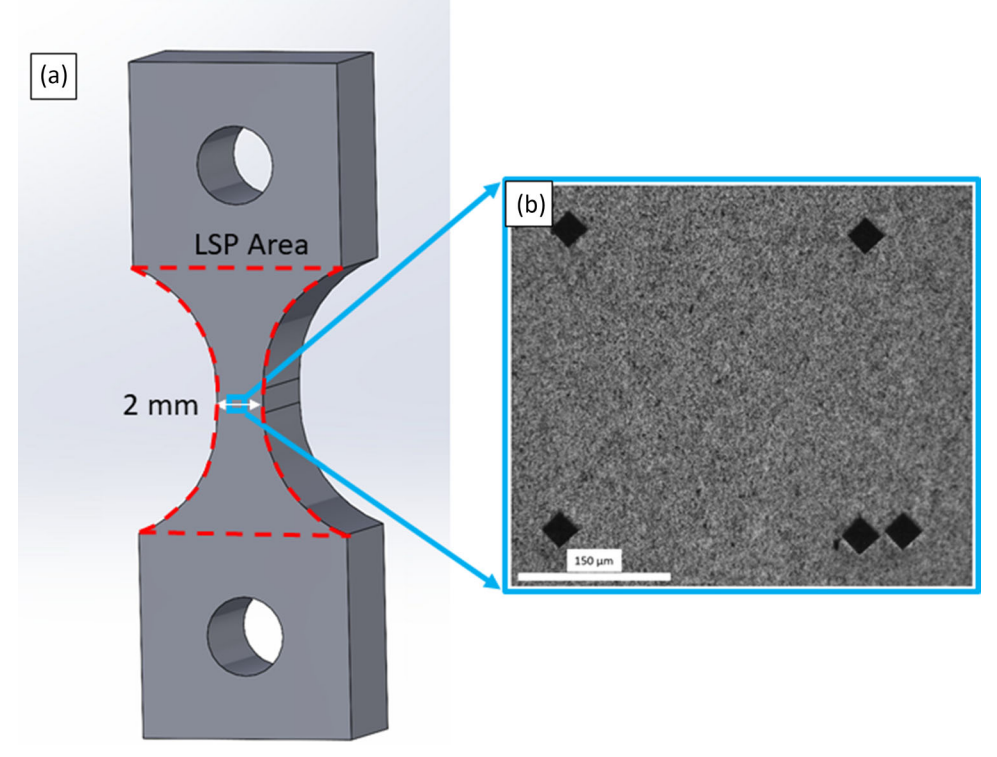


Fig. 2. (a) AlSi10Mg specimen geometry where the HRDIC area of interest is shown by the blue square, and the laser shock peening location is outlined in the dashed red line. (b) High-resolution speckle pattern with fiducial locating markers and air-blasted 1200 mesh aluminum oxide speckle pattern.

method. ^{49,51,52} For more detailed information on the contour method, see the work of Prime et al. ⁵³

Due to the continual remelting during the manufacturing process, AM components are known to have large amounts of residual stresses.^{54,55} Therefore, the initial residual stress analysis was conducted on a wrought sample to ensure that the given residual stress measurement would be from the FLSP process only. To ensure that the residual stress measurement had no edge effects, the FLSP process was performed in the center of square stock instead of entire specimen geometry. A wire EDM was used to cut all specimens to create a flat cutting surface. A cutting jig similar to what was detailed by Prime et al. was used to hold both sides of the specimen during the cutting process.⁵³ For measuring the surface heights of the cut samples, a Nanovea ST500 laser profilometer was used. The Nanovea ST500 created an output file that gave coordinates for each height measurement so that the entire cut surface of the specimen could be mapped in 15 μ m spacing. Before performing the FEA, a bivariate quadratic smoothing spine function was used in order to remove surface roughness from the data, similar to previous works. 49 The inverse of the resulting displacement surface was used as the initial displacement boundary condition for the FEA model. 53 The resulting out-of-plane stress on the cut surface was then saved and exported as the residual stress values from the FLSP process.

Strain-Controlled LCF

A series of strain-controlled fatigue experiments were conducted on an MTS Landmark 370.10 hydraulic load frame with a 100 kN load cell. To control the loading for the specified strain ranges, non-contacting virtual strain gauges were used via DIC. The length of the virtual extensometer was between 9 and 10 mm, and each end of the extensometer had DIC gauges of 35–45 pixels. Each virtual strain gauge was established at a zero load before the start of each test. Vic-Gauge from Correlated Solutions, Inc., was used for the strain measurements. All experiments were run at 2 Hz and at strain amplitudes that ranged from 0.05% to 0.4%. The total number of cycles to failure for specimens of all three layer heights was recorded for each experiment.

High-Resolution DIC Fatigue

Four high-resolution DIC fatigue experiments were conducted. The corresponding localized strain fields were overlayed with the electron backscatter diffraction (EBSD) maps of the area of interest. The following procedure will be detailed but an in-depth explanation of the process can be accessed from Carroll et al. ^{56,57} Before starting each test, the specimens were mechanically polished to a mirror finish starting with Buehler polishing pads,

increasing from 600 to 1200 grit, and then transitioning to three levels of polishing paste and ending with a colloidal silica solution. Before EBSD was performed, five fiducial markers were placed on the surface of the specimen, as seen in Fig. 2b. These fiducial markers are important for locating the area of interest when transitioning from the SEM/EBSD and optical microscopy during the fatigue experiments. The double marked corner gives orientation information for overlaying the results.

A Hitachi SU5000 SEM was used for the EBSD measurements. The acceleration voltage was 25 kV, and the measurement spacing was 1 μ m. The specimens were speckled after EBSD using a technique of air blasting 2.6–3.6-micron-sized aluminum oxide particles from Kramer Industries Inc. onto the surface, as show in Fig. 2b. ⁵⁸ By decreasing the field of view, the resolution of measurements was increased significantly allowing strain fields to be analyzed on a subgranular level. When comparing the resolution in the "Strain-controlled LCF" section to the resolution for HRDIC, the resolution improved from 15.38 μ m per pixel to 0.57 μ m per pixel, a reduction of 96%.

Stress-controlled fatigue experiments were performed on a horizontal 10 kN Psylotech load frame with an optical microscope mounted to capture images in situ throughout the fatigue experiment. Two sets of fatigue experiments were run at 2 Hz with a force amplitude of 1 kN for the first set of experiments (one as-built and one with FLSP) and subsequently at 875 N with pictures being taken every 250 cycles. For all DIC results, the initial reference frame was a picture taken initially with no load on the specimen. DIC was performed using VIC-2D from Correlated Solutions, Inc. A subset size of 65 pixels and a step size of 5 pixels were used for every analysis. Strain calculations were performed with Gaussian weights with a strain window of 5 pixels. The HRDIC experiments were analyzed with a spatial resolution of 32 μ m using the procedure outlined in Refs. 59 and 60. For overlapping the strain fields with the EBSD maps, MATLAB was used to align and scale the maps using the fiducial markers from EBSD processed through mtex and the DIC results.

RESULTS AND DISCUSSION

Residual Stress

The out-of-plane residual stresses from the cut plane were analyzed. The FEA results from the contour method for residual stress analysis can be seen in Fig. 3. The largest calculated compressive residual stress was 746 MPa, and depth of the compressive residual stresses zone was about 0.5 mm. These results agree with other reported results using the contour method and other forms of residual stress measurements. 21,23,24 As stated previously, the critical zone for gaseous pores has been characterized to be $< 100~\mu m.$ 3,17 With the depth of

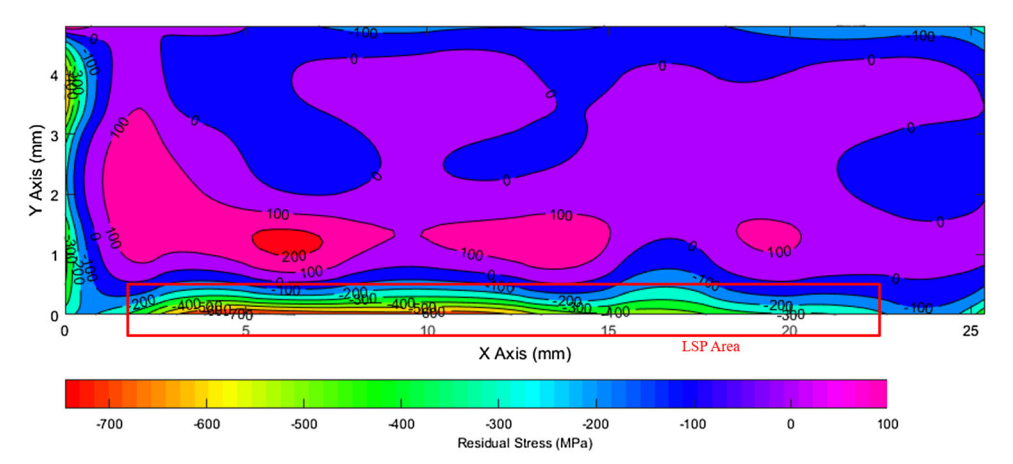


Fig. 3. Out-of-plane residual stress field for the femtosecond laser shock peening surface treatment using the contour method.

the compressive residual stress zone being about 0.5 mm, the compressive zone extended well beyond the critical pore region. Thus, it can be concluded that the critical pores that have been determined to be detrimental to the fatigue life will have a compressive residual stress surrounding them. Although understanding the magnitude of the residual stress is important for quantification purposes, due to the small sample size, the goal of this residual stress analysis was to ensure that the compressive residual stress zone penetrated deep enough to cover the critical pore zone.

EBSD Results

The EBSD results for a top, middle and bottom specimen can be seen in Fig. 4. The top (Fig. 4a) and bottom (Fig. 4c) specimens were in the non-treated condition, and the middle (Fig. 4b) specimen was treated with FLSP. The flower-like structure seen in all three EBSD maps is common to the AM process with corresponding large columnar grains and clustering of smaller grains near melt pool lines. 36,39,40,42,61 The build direction with respect to the images is out of plane; thus, the specimens are built such that the bottom specimen was printed first followed by the middle then top specimen. EBSD was performed on all three layers of specimens to identify any influences of build height. In addition, one FLSP-treated specimen was included to show that the treatment did not alter the microstructure. Table II shows the average grain size and aspect ratio for all three locations. The aspect ratio is defined as the long axis divided by the short axis of an ellipse fit to each grain. It is not unusual for the microstructure to change with respect to the build height, 62-64 influencing the performance of a specimen. 23,65,66 Minor differences were identified between the layer heights. The top layer had an average grain size of approximately 25 μm larger, fairly insignificant in coarse grained materials. The largest difference was in the aspect ratio between the bottom and top layers, but the

fatigue results discussed later will show that the change in microstructure did not play a major role in the fatigue life. The EBSD scans shown in Fig. 4 were used during the HRDIC overlaying analysis.

To ensure that there were stochastic pores within the material, XCT was performed on two middle specimens before FLSP. The results of the scan can be seen in Fig. 5. These specimens were printed using the manufacturer-recommended processing parameters, and although there was not a large amount of porosity in the specimens, the XCT images show that there were still pores throughout the specimens. In total, the samples had 136 and 149 pores for sample A and sample B, respectively. Of these pores, 27 pores in sample A and 38 pores in sample B were within the previously identified near-surface critical zone. This justifies that even under current ideal printing parameters, porous defects can be minimized but not removed from AM components. The stochastic pores within the critical zone were present, and although the pores were not characterized by size, the number of pores present indicated that there was a good probability that pores were present within the critical zone for all specimens.

Strain-Controlled LCF

With the microstructure for each layer within the block understood, the fatigue life was analyzed regarding layer height and with/without surface treatment. Figure 6 shows the fatigue life of AlSi10Mg samples for both the non-LSP and FLSP samples. From the non-LSP samples, labeled in Fig. 6 as top, middle and bottom specimens, the fatigue results indicate that the results were insensitive to specimen location within the build plate. At a strain amplitude of 0.2%, specimens failed within a range of 6724 cycles for non-LSP samples while the range for the FLSP samples was reduced to 1479 cycles. That is a reduction of 78% in scatter by applying the FLSP surface treatment. For both the non-LSP and FLSP samples, all three specimen

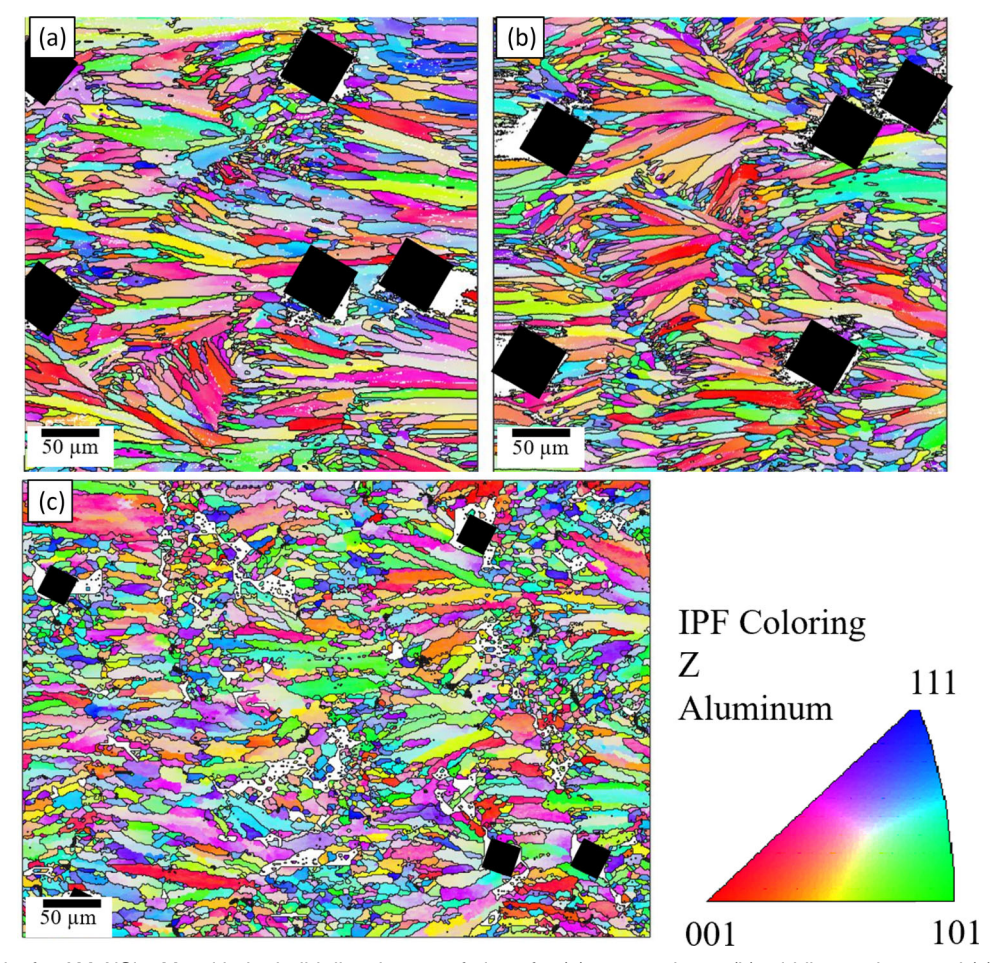


Fig. 4. EBSD results for AM AlSi10Mg with the build direction out of plane for (a) top specimen, (b) middle specimen and (c) bottom specimen. The black diamonds represent the locations of the fiducial markers for high-resolution experiments.

Table II. EBSD grain size and distribution for all three locations, top, middle and bottom, of an AM AlSi10Mg block

Location	Total number of grains	Average grain size (µm)	Standard deviation for grain size (µm)	Average aspect ratio (-)	
Top	1673	111	315	2.94	
Middle	2298	85	235	2.49	
Bottom	6330	88	237	1.77	

locations were used, which verified the reduction in scatter regardless of layer height.

After being treated by FLSP, specimens from all three layer heights were also tested at a 0.5% strain amplitude. The scatter showed a cycle range of 100,273 cycles, proportional to the scatter band width of the FLSP specimens tested at the 0.2% strain amplitude. Although the range of cycles to failure expanded, the scatter band remained consistent, matching the similar trend of improvement compared to the non-LSP samples at 0.2% strain amplitude. The major observation that the FLSP surface treatment did not extend the low cycle fatigue life of the AM specimens was

consistent with what has been shown in other studies. 68–72 More fatigue experiments are needed for probabilistic fatigue life predictions, but the initial results from this study show a promising enhancement in reducing scatter, increasing confidence in design and service life. The current study was focused on the same block of material, which minimized samples available, to minimize processing effects such as the known volatility because a multitude of factors for each build can lead to differing material properties. 18,48,65

Although the fatigue life was not increased in the low cycle fatigue realm, the scatter of the low cycle fatigue results was reduced when using a FLSP

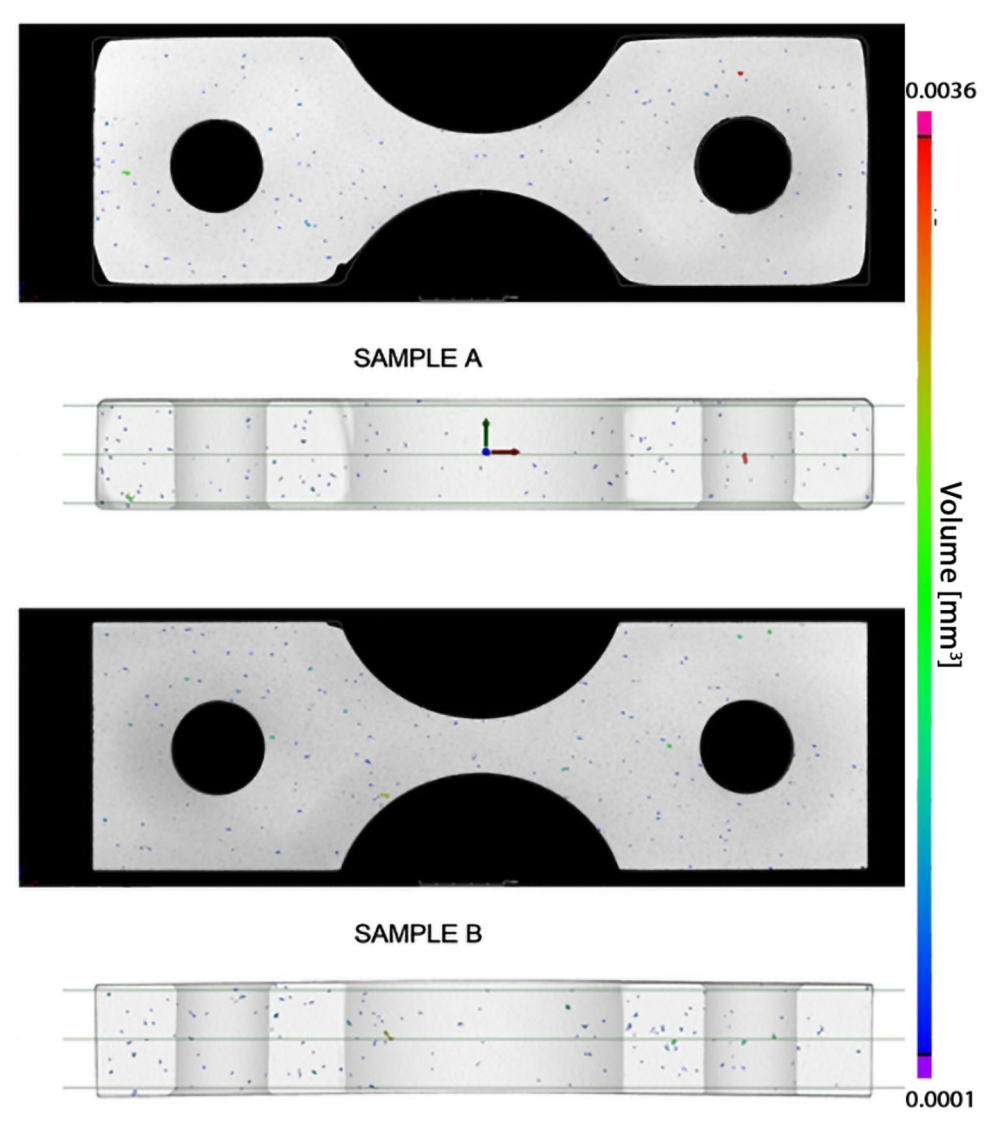


Fig. 5. XCT scans from two middle specimens of AM AlSi10Mg before FLSP.

surface treatment. In similar cases, the results were attributed to the compressive residual stress layer on the surface of the component creating a dense dislocation zone that resisted crack propagation. 68,69,73,74 In the referenced material about LSP, the materials used were wrought metals that lacked the signature defects present in AM metals, like the gaseous pores, and most of the wrought materials used were standardized. This means that the processing conditions were idealized after decades of improvement and minimized all external factors from batch to batch. This is different compared to the relatively newer AM processes that have been shown to produce different properties build to build and even within the same build.⁴⁴ It is hypothesized that the effect of stochastic pores near the surface that are inherent from the AM process was reduced when compressed with FLSP,

reducing premature crack initiation from porosity and resulting in less scatter in the fatigue life.

The residual stress on the LSP specimens caused the specimens to strain harden over the course of the fatigue life. Similar results were also seen for other wrought materials under the influence of surface treatments. 68,71,74 The change in material response was studied in depth by Altenberger et al. where they used TEM images to show the high dislocation density region near the surface appeared to suppress surface cracks and early small crack growth. 69 The high dislocation density region was shown to be 5 $\mu \rm m$ below the surface, and the critical pore distance was proposed to be $\geq 100~\mu \rm m$. Although the critical pore zone was at least 95 $\mu \rm m$, the compressive residual stress zone present within the material was shown to overlap with and exceed the entire critical pore zone. 69 Given that the FLSP

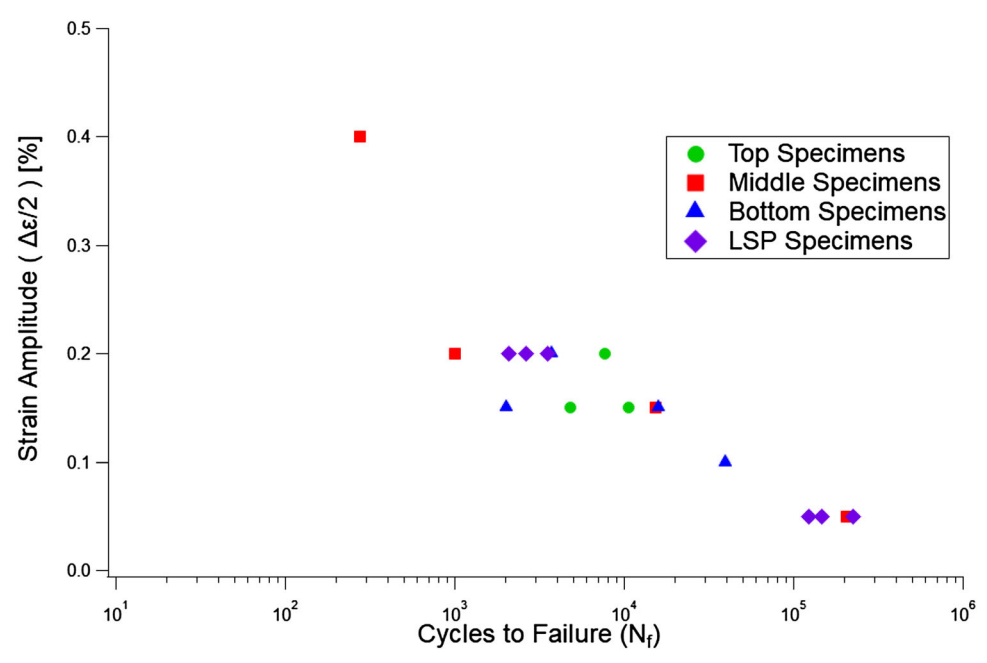


Fig. 6. Strain-controlled fatigue experiments of AlSi10Mg with strain amplitudes ranging from 0.05-0.4% for both untreated and FLSP samples.

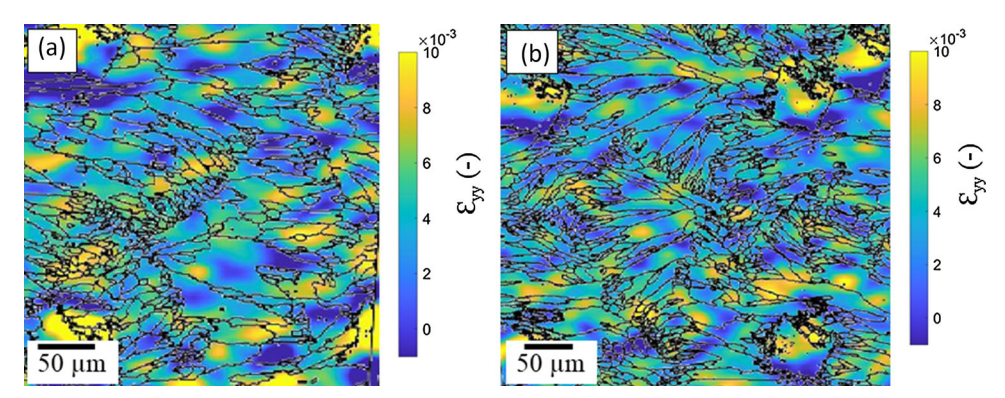


Fig. 7. HRDIC with grain boundaries at a stress amplitude of 875 N for (a) non-LSP specimen, (b) FLSP specimen.

system used in this experiment created a compressive residual stress zone that encompassed the detrimental near surface pores from the AM process, the low cycle fatigue life became less sensitive to the critical pores which created a more uniform material response.

High-Resolution DIC Fatigue

The strain field for an as-built and FLSP specimen within 500 cycles of fracture can be seen in Fig. 7. The average strain within each grain, excluding the grains that have edge effects from the fiducial markers, was calculated. Table III shows the average strain result within the grains for all four HRDIC experiments. The range of average strain was reduced by using the FLSP process in both force amplitude cases: the 1 kN amplitude case saw a reduction of 71% and the 0.875 kN amplitude case saw a reduction of 44%.

Due to the large forces and relatively short life after crack initiation before ultimate failure, the crack propagation was not captured in the area of interest. The strain fields in Fig. 7 show that the non-LSP case has slightly higher localized strain locations. When coupled with the data in Table III, the results show that the compressive stress region created from FLSP interacts with the stress raisers present on the surface, or below the surface, to create a more homogeneous strain field.

The fatigue life showed similar traits to those of the strain-controlled fatigue experiments where there was no significant improvement of fatigue life. The reduction in scatter could be attributed to the reduction in average strain per grain range. The compressive stress region, which has been shown to suppress surface cracks and small crack growth in wrought metals, could also reduce the criticality of the pores near the surface of AM components. ^{18,69,75} Given the ability of the residual stress region to

Specimen number	Force amplitude (kN)	Total number of grains	Mean average strain (%)	Maximum average strain (%)	Minimum average strain (%)	Range of average strain (%)
FLSP run 1	1	5,267	0.51	1.03	-0.14	1.17
Non-LSP	1	6,333	0.29	2.24	$-\ 1.76$	4.0
run 1						
FLSP run 2	0.875	3,466	0.38	0.61	0.05	0.56
Non-LSP	0.875	1,445	0.42	0.81	- 0.19	1.0

Table III. The mean, maximum, minimum and range for the average strain within a grain value over all four experiments at two different loading conditions

suppress surface crack initiation, the ability of that same residual stress region to suppress the stress concentrations between a gaseous pore and outer surface could also be extrapolated. The suppression of the stress concentration around the pore by way of surface treatment can be furthered by the reduction of the average strain range for the FLSP samples compared to as-built samples. The maximum and minimum average strains within a grain for the non-LSP case are hypothesized to be the locations of the detrimental subsurface pores. All fracture surfaces were analyzed after failure, and all fracture surfaces had gaseous pores present on the surface. Given that the HRDIC was performed in the area were the specimens fractured, this further supports the presented hypothesis. When comparing the non-LSP and FLSP specimens, the FLSP specimens have reduced maximum and minimum average strain values showing that the detrimental pores have a reduced localized stress raiser. This increase of the homogeneity of the strain field would lend to a more consistent fatigue life given that strain fields with stress concentrations are prone to early fatigue failure due to the increased local stresses initiating fatigue cracks. ¹⁵

With these gaseous pores being stochastic in nature, consistent material responses regarding fatigue make qualifying AM materials a challenge. The instances where AM components have been able to successfully meet qualification standards for use in mass production runs is limited. 76,77 addition, all print runs in these studies were conducted on the same production component that had considerable, focused upfront testing with constant quality control measures. Requiring each component to undergo such an extensive testing procedure eliminates the advantage of AM with its ability to rapidly prototype and create low production runs. With changing geometries and processing parameters comes differing material structures, which leads to complex material responses. The National Institute of Standards and Technology (NIST) hosted a workshop on the behavior of AM components, and one of their main conclusions was

that standardizations were needed on multiple fronts.⁷⁷ The first front was on the AM processing side, while the second front was on the material qualification side. There was a lack agreement on whether traditional qualification standards were desired or if there needed to be a new standard set forth by one of the regulatory agencies to help meet the needs of AM components. This need stemmed from the inherent different behaviors of AM components and wrought components. This research was a step forward in identifying a way to standardize AM components. The introduction of FSLP treatments to reduce fatigue scatter provides the potential to be able to qualify components regardless of the combination of materials, AM machines and complex geometries. The decrease in variation leads to a more accurate prediction of the behavior and confidence in the part performance.

CONCLUSION

Using an FLSP treatment on AM AlSi10Mg samples during fatigue loading, the major conclusions reached were:

- 1. The FLSP surface treatment was able to penetrate deep enough to create a compressive residual stress zone that covered the entire critical pore zone.
- 2. The FLSP did not extend the low cycle fatigue life of the AM specimens. However, the surface treatment decreased the fatigue scatter for two given amplitudes.
- 3. Using HRDIC techniques, the range of the average strain within a grain was reduced by up to 71% using the FLSP surface treatment. The reduction in fatigue scatter was attributed to the reduction in the average strain range.

The decrease in fatigue scatter is important for material characterization of AM materials. For material specifications to be met or created, there is a level of consistency that must be met within that material. Typically, defects result in undesirable or unusable material, but with AM it is currently an inherent byproduct. The use of a FLSP

surface treatment to decrease the fatigue scatter presents an opportunity for standardizing AM materials.

ACKNOWLEDGEMENTS

This material is based upon work partially supported by the National Science Foundation under grant no. 1829008. The material was supplied by Dr. Jay Carroll from Sandia National Laboratories. The FLSP work was partially supported by the Nation Science Foundation under grant no. 1762581. All electron microscopy work was conducted with the assistance of Dr. Laxmikant Saraf from Clemson's Advanced Materials Research Laboratory.

CONFLICT OF INTEREST

On behalf of all authors, the corresponding author states that there is no conflict of interest.

REFERENCES

- P. Li, D.H. Warner, A. Fatemi, and N. Phan, Int. J. Fatigue 85, 130 (2016).
- L. Sheridan, O.E. Scott-Emuakpor, T. George, and J.E. Gockel, Mater. Sci. Eng. A 727, 170 (2018).
- S. Romano, A. Brückner-Foit, A. Brandão, J. Gumpinger, T. Ghidini, and S. Beretta, Eng. Fract. Mech. 187, 165 (2018).
- S.H. Khajavi, J. Partanen, and J. Holmström, Comput. Ind. 65, 50 (2014).
- A.B. Spierings, T.L. Starr, and K. Wegener, Rapid Prototyp. J. 19, 88 (n.d.).
- 6. T.J. Horn, and O.L.A. Harrysson, Sci. Prog. 95, 255 (2012).
- D. Bourell, J.P. Kruth, M. Leu, G. Levy, D. Rosen, A.M. Beese, and A. Clare, CIRP Ann. 66, 659 (2017).
- 8. M. Benedetti, V. Fontanari, M. Bandini, F. Zanini, and S. Carmignato, *Int. J. Fatigue* 107, 96 (2018).
- 9. M. Tang and P.C. Pistorius, Int. J. Fatigue 125, 479 (2019).
- J.N. Domfang Ngnekou, Y. Nadot, G. Henaff, J. Nicolai, W.H. Kan, J.M. Cairney, and L. Ridosz, *Int. J. Fatigue* 119, 160 (2019).
- E. Wycisk, A. Solbach, S. Siddique, D. Herzog, F. Walther, and C. Emmelmann, in *Phys. Procedia* (Elsevier B.V., 2014), pp. 371–378.
- 12. Z. Jin, Z. Zhang, and G.X. Gu, Adv. Intell. Syst. 2, 1900130 (2020).
- T. Craeghs, F. Bechmann, S. Berumen, and J.P. Kruth, Phys. Procedia 5, 505 (2010).
- A. Leicht, U. Klement, and E. Hryha, *Mater. Charact.* 143, 137 (2018).
- S. Suresh, Fatigue of Materials, 2nd edn. (Cambridge University Press, Cambridge, 2004).
- P. Li, D.H. Warner, J.W. Pegues, M.D. Roach, N. Shamsaei, and N. Phan, *Int. J. Fatigue* 126, 284 (2019).
- R. Shrestha, N. Shamsaei, M. Seifi, and N. Phan, Addit. Manuf. 29, 100807 (2019).
- R. Biswal, X. Zhang, A.K. Syed, M. Awd, J. Ding, F. Walther, and S. Williams, *Int. J. Fatigue* 122, 208 (2019).
- 19. A. Yadollahi and N. Shamsaei, *Int. J. Fatigue* 98, 14 (2017).
- W. Schneller, M. Leitner, S. Springer, F. Grün, and M. Taschauer, J. Manuf. Mater. Process. 3, 16 (2019).
- M. Benedetti, E. Torresani, M. Leoni, V. Fontanari, M. Bandini, C. Pederzolli, and C. Potrich, J. Mech. Behav. Biomed. Mater. 71, 295 (2017).
- C.A. Rodopoulos, J.S. Romero, S.A. Curtis, E.R. De Los Rios, and P. Peyre, J. Mater. Eng Perform 12, 414 (2003).
- N.E. Uzan, S. Ramati, R. Shneck, N. Frage, and O. Yeheskel, *Addit. Manuf.* 21, 458 (2018).

- S. Luo, W. He, K. Chen, X. Nie, L. Zhou, and Y. Li, J. Alloys Compd. 750, 626 (2018).
- W. Jia, Q. Hong, H. Zhao, L. Li, and D. Han, *Mater. Sci. Eng. A* 606, 354 (2014).
- X.C. Zhang, Y.K. Zhang, J.Z. Lu, F.Z. Xuan, Z.D. Wang, and S.T. Tu, *Mater. Sci. Eng. A* 527, 3411 (2010).
- E. Liverani, Y. Li, A. Ascari, X. Zhao, and A. Fortunato, Procedia CIRP 108, 77 (2022).
- Y. Li, Z. Ren, X. Jia, W. Yang, N. Nassreddin, Y. Dong, C. Ye, A. Fortunato, and X. Zhao, Manuf. Lett. 27, 26 (2021).
- T. Sano, T. Eimura, R. Kashiwabara, T. Matsuda, Y. Isshiki,
 A. Hirose, S. Tsutsumi, K. Arakawa, T. Hashimoto, K. Masaki, and Y. Sano, J. Laser Appl. 29, 012005 (2017).
- 30. J.D. Majumdar, E.L. Gurevich, R. Kumari, and A. Ostendorf, Appl. Surf. Sci. 364, 133 (2016).
- R. Le Harzic, N. Huot, E. Audouard, C. Jonin, P. Laporte, S. Valette, A. Fraczkiewicz, and R. Fortunier, Appl. Phys. Lett. 80, 3886 (2002).
- T. Kawashima, T. Sano, A. Hirose, S. Tsutsumi, K. Masaki, K. Arakawa, and H. Hori, J. Mater. Process. Technol. 262, 111 (2018).
- Y. Sano, K. Masaki, T. Gushi, and T. Sano, *Mater. Des.* 36, 809 (2012).
- Y. Bai, H. Wang, S. Wang, Y. Huang, Y. Chen, W. Zhang, A. Ostendorf, and X. Zhou, *Appl. Surf. Sci.* 569, 151118 (2021).
- X. Kai Meng, H. Wang, W. Sheng Tan, J. Cai, J. Zhong Zhou, and L. Liu, Surf. Coatings Technol. 391, 125698 (2020)
- Y. Wang, R. Chen, X. Cheng, Y. Zhu, J. Zhang, and H. Wang, J. Mater. Sci. Technol. 35, 403 (2019).
- M.D. Sangid, G.J. Pataky, H. Sehitoglu, R.G. Rateick, T. Niendorf, and H.J. Maier, Acta Mater. 59, 7340 (2011).
- Y. Zhai, H. Galarraga, and D.A. Lados, *Eng. Fail. Anal.* 69, 3 (2016).
- P.D. Nezhadfar, E. Burford, K. Anderson-Wedge, B. Zhang, S. Shao, S.R. Daniewicz, and N. Shamsaei, *Int. J. Fatigue* 123, 168 (2019).
- D. Tomus, Y. Tian, P.A. Rometsch, M. Heilmaier, and X. Wu, Mater. Sci. Eng. A 667, 42 (2016).
- D. Zhang, W. Niu, X. Cao, and Z. Liu, Mater. Sci. Eng. A 644, 32 (2015).
- 42. S. Cheruvathur, E.A. Lass, and C.E. Campbell, *JOM* 68, 930 (2016)
- A. Yegyan Kumar, Y. Bai, A. Eklund, and C.B. Williams, Addit. Manuf. 24, 115 (2018).
- C.M. Laursen, S.A. DeJong, S.M. Dickens, A.N. Exil, D.F. Susan, and J.D. Carroll, *Mater. Sci. Eng. A* 795, 139922 (2020)
- P. Yang, L.A. Deibler, D.R. Bradley, D.K. Stefan, and J.D. Carroll, J. Mater. Res. 33, 4040 (2018).
- B.A. Smith, C.M. Laursen, J. Bartanus, J.D. Carroll, and G.J. Pataky, *Exp. Mech.* 61, 685 (2021).
- C.B. Finfrock, A. Exil, J.D. Carroll, and L. Deibler, Metallogr. Microstruct. Anal. 7, 443 (2018).
- C.M. Laursen, S.A. DeJong, S.M. Dickens, A.N. Exil, D.F. Susan, and J.D. Carroll, *Mater. Sci. Eng. A* 795, 139922 (2020).
- M.B. Prime, R.J. Sebring, J.M. Edwards, D.J. Hughes, and P.J. Webster, *Exp. Mech.* 44, 176 (2004).
- M.B. Prime and A.L. Kastengren, in Conf. Proc. Soc. Exp. Mech. Ser. (Springer New York LLC, 2011), pp. 233–250.
- P. Pagliaro, M.B. Prime, H. Swenson, and B. Zuccarello, Exp. Mech. 50, 187 (2010).
- G.S. Schajer, Practical Residual Stress Measurement Methods (John Wiley & Sons, Ltd, Chichester, UK, 2013).
- M. B. Prime, M. R. Hill, A. T. DeWald, R. J. Sebring, V. R. Dave, and M. J. Cola, in ASM Proc. Int. Conf. Trends Weld. Res. (ASM International, 2002), pp. 891–896.
- 54. W.E. Frazier, J. Mater. Eng. Perform. 26, 1917 (2014).
- J.J. Lewandowski and M. Seifi, Annu. Rev. Mater. Res. 46, 151 (2016).
- J.D. Carroll, W. Abuzaid, J. Lambros, and H. Sehitoglu, Int. J. Fatigue 57, 140 (2013).

- J. Carroll, W. Abuzaid, J. Lambros, and H. Sehitoglu, Rev. Sci. Instrum. 81, 083703 (2010).
- 58. G.J. Pataky, and H. Sehitoglu, Exp. Mech. 55, 53 (2015).
- 59. P. Reu, Exp. Tech. 39, 1 (2015).
- E.M.C. Jones and M.A. Iadicola (Eds.), Int. Digit. Image Correl. Soc. (2018). https://doi.org/10.32720/idics/gpg.ed1/pr int.format.
- M. Awd, S. Siddique, J. Johannsen, C. Emmelmann, and F. Walther, Int. J. Fatigue 124, 55 (2019).
- Z. Wang, T.A. Palmer, and A.M. Beese, Acta Mater. 110, 226 (2016).
- K.L. Johnson, T.M. Rodgers, O.D. Underwood, J.D. Madison, K.R. Ford, S.R. Whetten, D.J. Dagel, and J.E. Bishop, *Comput. Mech.* 61, 559 (2018).
- B.E. Carroll, T.A. Palmer, and A.M. Beese, *Acta Mater.* 87, 309 (2015)
- A. Mussatto, R. Groarke, R.K. Vijayaraghavan, C. Hughes, M.A. Obeidi, M.N. Doğu, M.A. Yalçin, P.J. McNally, Y. Delaure, and D. Brabazon, *Mater. Today Commun.* 30, 103209 (2022).
- A. Soltani-Tehrani, J. Pegues, and N. Shamsaei, Addit. Manuf. 36, 101398 (2020).
- M. Sangid, Fatigue Modeling of U720 A Multi-scale Approach in Understanding Grain Boundary Effects on Crack Initiation, Doctoral dissertation, University of Illinois at Urbana-Champaign (2010).
- V. Pandey, K. Chattopadhyay, N.C. Santhi Srinivas, and V. Singh, Int. J. Fatigue 103, 426 (2017).
- I. Altenberger, R.K. Nalla, Y. Sano, L. Wagner, and R.O. Ritchie, Int. J. Fatigue 44, 292 (2012).
- S.A.A. Shams, G. Jang, J.W. Bae, A. Amanov, H.S. Kim, T. Lee, and C.S. Lee, *Mater. Sci. Eng. A* 853, 143724 (2022).

- C.S. Kumar, K. Chattopadhyay, V. Singh, and G.S. Mahobia, Mater. Today Commun. 25, 101576 (2020).
- A. Bag, D. Delbergue, J. Ajaja, P. Bocher, M. Lévesque, and M. Brochu, *Int. J. Fatigue* 130, 105274 (2020).
- H. Zhang, Z. Cai, J. Chi, R. Sun, Z. Che, H. Zhang, and W. Guo, J. Alloys Compd. 887, 161427 (2021).
- J. Zhou, D. Retraint, Z. Sun, and P. Kanouté, Surf. Coatings Technol. 349, 556 (2018).
- K. Yang, Q. Huang, Q. Wang, and Q. Chen, Int. J. Fatigue 136, 105580 (2020).
- M. Seifi, A. Salem, J. Beuth, O. Harrysson, and J.J. Lewandowski, *Jom* 68, 747 (2016).
- 77. N. Hrabe, N. Barbosa, S.R. Daniewicz, and N. Shamsaei, Findings from the NIST/ASTM Workshop on Mechanical Behavior of Additive Manufacturing Components, Advanced Manufacturing Series (NIST AMS) (National Institute of Standards and Technology, Gaithersburg, MD, 2016).

Publisher's Note Springer Nature remains neutral with regard to jurisdictional claims in published maps and institutional affiliations.

Springer Nature or its licensor (e.g. a society or other partner) holds exclusive rights to this article under a publishing agreement with the author(s) or other rightsholder(s); author self-archiving of the accepted manuscript version of this article is solely governed by the terms of such publishing agreement and applicable law.